


Article

Improvement in Tribological Properties of Cr₁₂MoV Cold Work Die Steel by HVOF Sprayed WC-CoCr Cermet Coatings

Sheng Hong ^{1,*} , Yuping Wu ^{1,*}, Bo Wang ¹ and Jinran Lin ^{2,3}

¹ College of Mechanics and Materials, Hohai University, 8 Focheng West Road, Nanjing 211100, China; 181608010027@hhu.edu.cn

² College of Engineering, Nanjing Agricultural University, 40 Dianjiangtai Road, Nanjing 210031, China; linjinran@njau.edu.cn

³ Jiangsu Jinxiang Transmission Equipment Co., Ltd., 1 Qinglonghu Road, Huaian 223001, China

* Correspondence: hongsheng@hhu.edu.cn (S.H.); wuyuping@hhu.edu.cn (Y.W.)

Received: 29 October 2019; Accepted: 3 December 2019; Published: 4 December 2019



Abstract: The main objective of this study was to develop an efficient coating to increase the wear resistance of cold work die steel at different temperatures. The microstructures of high-velocity oxygen-fuel (HVOF)-sprayed WC-CoCr coatings were evaluated using scanning electron microscopy (SEM) and transmission electron microscopy (TEM). The effect of temperature on the tribological properties of the coatings and the reference Cr₁₂MoV cold work die steel were both investigated by SEM, environmental scanning electron microscopy (ESEM), X-ray diffraction (XRD), and a pin-on-disk high-temperature tribometer. The coating exhibited a significantly lower wear rate and superior resistance against sliding wear as compared to the die steel at each test temperature, whereas no major differences in terms of the variation tendency of the friction coefficient as a function of temperature were observed in both the coatings and the die steels. These can be attributed to the presence of nanocrystalline grains and the fcc-Co phase in the coating. Moreover, the wear mechanisms of the coatings and the die steels were compared and discussed. The coating presented herein provided a competitive approach to improve the sliding wear performance of cold work die steel.

Keywords: sliding wear; cold work die steel; HVOF; WC-CoCr; cermet

1. Introduction

Friction, as one of the major sources of energy dissipation between the contact surfaces, is the main cause of wear and is also a common phenomenon in many industries such as rolling, packaging and mineral processing, where cold work die steel is widely used [1]. Most engineering components require the application of advanced materials that are resistant to wear in order to prevent or decrease material losses due to wear, to reduce the downtime of the equipment, and to increase efficiency and component quality. In order to meet these requirements, various metals [2], ceramics [3], and surface materials [4,5] with a unique combination of corrosion and wear resistance and high-temperature stability are being investigated and considered as effective methods to tailor the properties of engineering components [4–8]. In particular, surface technologies have been applied to a wide variety of materials without the necessity of using expensive and time-consuming heat treatments or alloying techniques, which can significantly change surface properties and may beneficially enhance the wear resistance of engineering materials [6,7]. As one of the most commonly-used surface coating technologies, thermal spraying has played a major role in the development of solutions for new technological problems as well as in the understanding of friction and wear mechanisms [8–10].

Ceramic–metal (i.e., cermet) is formed by at least a hard and a tough metallic binder phase to achieve specific properties for particular applications as a result of its exceptional toughness, high mechanical strength, corrosion and wear resistance [11]. For carbide cermet coatings, the chemical stability and oxidation resistance during the spraying process, which depend on chemical composition, microstructure, and surface condition of raw powders, should be improved when coming to the most demanding applications. Besides, the proper selection of thermal spraying techniques and the optimization of spraying process are also important steps [12–14]. High-velocity oxygen-fuel (HVOF) spraying is an option for these sorts of problems, as well as for the suppression or reduction of the decarburization and dissolution of carbides. In recent decades, considerable attempts have been devoted to improving the mechanical and wear properties of HVOF-sprayed WC-based cermet coatings through the proper choice of carbide size, binder phases and processing parameters [15–20]. Yang et al. [15] found that a higher wear rate is found with increasing carbide size for HVOF-sprayed WC-Co coatings. Meanwhile, Wesmann and Espallargas [16] investigated the tribological behaviors of HVOF-sprayed WC-CoCr coatings containing different carbide sizes and found that the effect of primary carbide size on friction and wear is marginal and somewhat inconsistent. Bolelli et al. [18] compared the dry sliding wear behaviors of HVOF-sprayed WC-(W,Cr)₂C–Ni and WC-CoCr coatings. It was found that the WC-(W,Cr)₂C–Ni coating exhibited a better wear resistance than the WC-CoCr coating, particularly at higher temperatures. Qiao et al. [20] reported that the hardest and toughest WC-Co coatings with superior tribological performance are obtained with a hot, neutral flame during the HVOF spraying process. Furthermore, the addition of Al into an HVOF-sprayed nanostructured WC-12Co coating is an effective method to enhance wear resistance [21]. However, till now, there is only limited works focus on sliding wear of HVOF-sprayed WC-based coatings at different temperatures [22,23]. Despite a high volume of published work, the high temperature wear properties of HVOF-sprayed WC-CoCr coatings have not been entirely understood.

In the past, the authors have demonstrated that HVOF-sprayed WC-CoCr coatings exhibit superior tribological properties as compared to the Cr12MoV cold work die steel at different loads, owing to the presence of a soft binder and a homogeneous dispersion of fine WC grains within the coating [24]. To our knowledge, there is still lack of systematic research on the relationship between detailed microstructures and sliding wear properties of HVOF-sprayed WC-CoCr coatings at different temperatures. The present study aimed to discover the effect of temperature on the sliding wear behavior of the WC-CoCr coating and to illustrate the dry sliding wear mechanisms at different temperatures in relation to the microstructures.

2. Experimental Procedure

Commercially available WC-CoCr cermet powder (Large Solar Thermal Spraying Material Co. Ltd, Chengdu, China) with a particle size of 15–45 μm was used for HVOF spraying in this study. The nominal composition of the cermet powder was, by wt. %: 4.0 Cr, 10.0 Co, 5.3 C, and 80.7 W. The WC-CoCr coating was deposited on Cr12MoV cold work die steel substrates with a thickness of approximately 200 μm by using an HVOF spray system (Praxair Tafa-JP8000, Danbury, CT, USA). Before spraying, the substrates were degreased with acetone in an ultrasonic bath, dried in hot air, and then adequately sandblasted with alumina (550 μm). The deposition of the coatings was conducted at the following conditions: a kerosene flow rate of 0.38 $\text{L}\cdot\text{min}^{-1}$ (standard liter per minute (SLPM)), oxygen flow rate of 897 $\text{L}\cdot\text{min}^{-1}$, spray distance of 300 mm, argon carrier gas flow rate of 10.86 $\text{L}\cdot\text{min}^{-1}$, powder feed rate of 50 $\text{g}\cdot\text{min}^{-1}$, and spray gun speed of 280 $\text{mm}\cdot\text{s}^{-1}$.

A scanning electron microscopes (SEM, Hitachi S-3400N, Tokyo, Japan) equipped with an energy dispersive spectroscope (EDS, EX250), alongside a high-resolution transmission electron microscope (HRTEM, JEOL JEM-2100F, Tokyo, Japan) were utilized to characterize the microstructures of the coating. Specimens for the TEM examination were prepared by grinding, polishing, mechanical dimpling, and argon ion milling to achieve electron transparency. The porosity of the coating was

calculated by randomly using an image analyzer on 20 optical microscopy (OM, Olympus BX51M, Tokyo, Japan) images with a magnification of 500 from polished cross sections of the coating.

Dry sliding friction and wear tests were conducted on a commercially available, pin-on-disk high-temperature tribometer (Beilun MG-2000, Zhangjiakou, China) according to standard ASTM G99-05 [25]. Before the test, all coating and die steel specimens were grinded by 240#, 400#, 600#, 800#, 1000#, 1500# and 2000# SiC abrasive papers, polished by 2.5 and 0.5 μm diamond pastes, cleaned in an ultrasonic bath with acetone, and subsequently dried in hot air. The average surface roughness (R_a) values of the specimens were 0.02 μm . In the test, the upper pin of Al_2O_3 ball with a diameter of 6 mm as the friction counterpart was stationary, while the counterface disk with a diameter of 45 mm and a thickness of 7 mm was rotated. The mating materials were HVOF-sprayed WC-CoCr coatings and Cr12MoV cold work die steel. Dry sliding tests were performed in air at room temperature (RT), 200 °C and 500 °C. The relative humidity varied between 35% and 55%. A normal load of 50 N and a sliding velocity of 0.9 $\text{m}\cdot\text{s}^{-1}$ for 30 min were applied. The frictional moments were consistently recorded by a computer. After the test, the R_a values and the wear tracks of all coating and die steel specimens were measured by a profile and roughness tester (Taiming JB-4C, Shanghai, China). The wear rate was calculated by dividing the volume loss by load and sliding distance. The morphologies of worn surface of the coatings were examined by SEM and EDS. The surfaces of the samples inside the wear tracks were further investigated by X-ray diffraction (XRD, Bruker D8-Advanced, Karlsruhe, Germany) with $\text{Cu K}\alpha$ radiation ($\lambda = 1.54 \text{ \AA}$) and step 0.02° operated at 40 kV and 40 mA in order to characterize the structure of the oxide scale that was formed at the various testing temperatures. The XRD patterns were taken with a beam spot size of 0.4 mm \times 2 mm, ensuring the focus of XRD optics and considerable diffraction intensity on the wear tracks. The worn surfaces of the Cr12MoV cold work die steel were characterized by environmental scanning electron microscopy (ESEM, Philips XL30, Hillsboro, Holland). Tests were conducted at least thrice for each condition to ensure the repeatability and reliability of the reported data.

3. Results and Discussion

3.1. Microstructural Analysis of WC-CoCr Coatings

Our previous studies [26,27] have shown that conventional WC-CoCr coatings can be successfully synthesized by HVOF spraying technology and an optimal spray parameter can be obtained. The coating was mainly composed of WC, W_2C and an amorphous phase. Figure 1 shows the typical cross-sectional morphologies of the coating deposited on the AISI 1045 steel substrate. This is revealed from the overall view shown in Figure 1a, which shows that the coating possessed a dense microstructure and the interface of the coating and substrate was compact without obvious stripping. The thickness value was about 200 μm for the coating. As shown in Figure 1b, few internal defects such as pores and microcracks were observed. The coating had a low porosity value of 0.77%, resulting from high flame velocity and low flame temperature of the HVOF spraying process, which restrains decarburization [27]. There was a homogeneous distribution of tungsten carbide grains, as shown in the magnified image of the rectangular frame in Figure 1b. Additionally, inter-lamellar oxidation is indicated by yellow arrow in Figure 1c, which may have been due to the reaction between tungsten and oxygen that came from the spraying chamber [28,29].

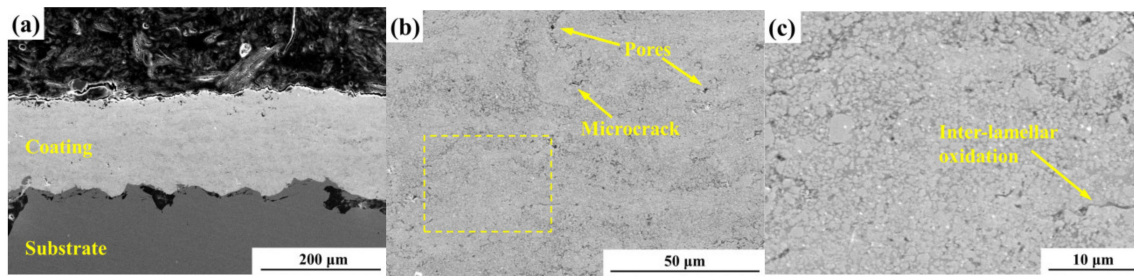


Figure 1. SEM images of a transverse section of the high-velocity oxygen-fuel (HVOF)-sprayed WC-CoCr coating: (a) an overall view morphology; (b) pores and microcracks; (c) a magnification of the rectangular frame in (b).

TEM and HRTEM images illustrating the detailed microstructure of the coating are shown in Figure 2. From Figure 2a, it can be seen that nanocrystalline grains were randomly oriented in the amorphous matrix and could be observed to be about 10 nm in size. The composition of amorphous matrix was Co–W–C, which was due to the high cooling rate of the splats. This is similar to phenomenon reported by Stewart et al. [30] and Li et al. [31]. According to the HRTEM image and selected area electron diffraction (SAED) pattern shown in Figure 2b,c, the nanocrystalline grains with an interplanar distance of 0.23 nm grew in parallel to the [100] zone axis, which corresponded to the W_2C phase. On the one hand, the size of nanocrystalline grains in the nanometer range was due to the presence of the amorphous phase, which can hinder grain growth during the coating process [32]. On the other hand, the formation of the nanocrystalline grains in the coating may lead to the enhancement of mechanical properties as a result of dispersion strengthening. A similar result was also observed by Lee et al. [33]. It is possible that the nanocrystalline/amorphous structure formed as a result of the solid state transformation and partial crystallization of the amorphous structure induced by the preferred oxidation on the in-flight particles surface and the thermal fluctuation from the subsequent splats [34,35]. The TEM analysis performed on the coating also indicated the presence of the fcc-Co phase, as shown in Figure 2d. The corresponding SAED pattern is shown in Figure 2e, which indicates that the Co phase was indexed to a face-centered cubic structure with the incident beam parallel to the zone axis of [320]. Human et al. [36] reported that compared to the hcp-Co phase, the fcc-Co phase is expected to be thermodynamically more stable. Hence, the presence of the fcc-Co phase is beneficial to the wear resistance of a coating at high temperatures.

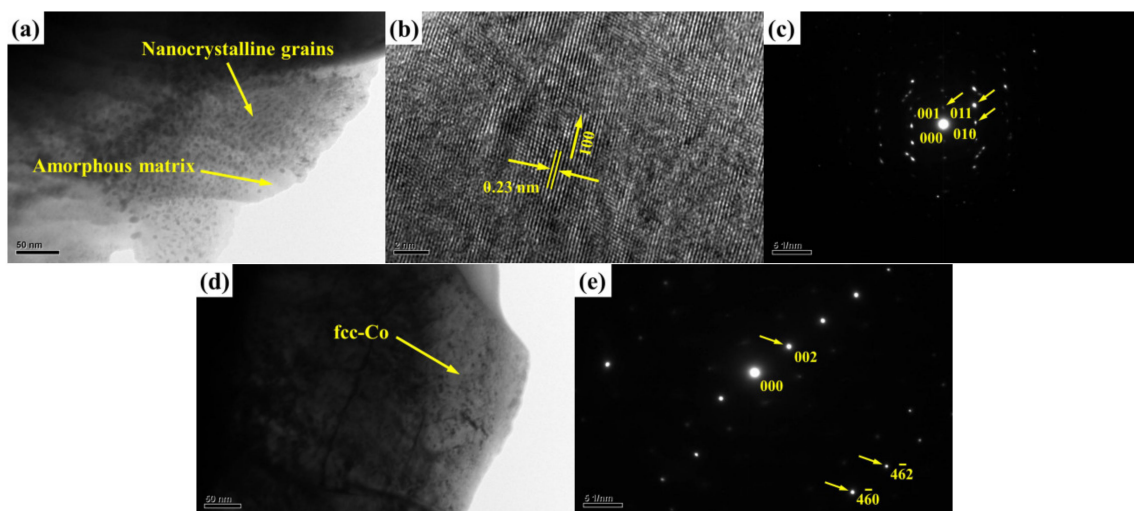


Figure 2. TEM images of typical microstructure of the HVOF-sprayed WC-CoCr coating: (a) a region of nanocrystalline grains and amorphous matrix; (b) high-resolution transmission electron microscopy (HRTEM) image of the nanocrystalline grain; (c) selected area electron diffraction (SAED) pattern of the W_2C phase; (d) a region of fcc-Co; and (e) SAED pattern of the fcc-Co phase.

3.2. Friction and Wear Properties

The friction coefficients data were continuously recorded by the high-temperature tribometer over a sliding time of 30 min. The typical friction coefficients of the HVOF-sprayed WC-CoCr coatings and Cr12MoV cold work die steel at different temperatures are shown in Figure 3a,b, respectively. It can be seen that all of the tests experienced a running-in period followed by a gradual stabilization in the friction coefficient value, which is consistent with the literature [37,38]. In all cases, the friction coefficient value was initially low and subsequently attained a steady state. This can be attributed to the evolution of tribo-oxidation products between the asperity contact of the tribopair at an early stage and the severe micro-fracture and subsequent pull-out of grains at a later stage of sliding [39]. Moreover, the fluctuation of the friction coefficient and the running-in period both decreased in duration with the increasing temperature, probably due to the lower initial resistance to the conformation between the two sliding surfaces as a result of the formation of larger amounts of the oxide films with lubricating properties at higher temperatures. This also suggests that there was a more efficient activation of wear protection processes at higher temperatures, which can be attributed to the more uniform distribution of the lubricating oxides over the wear track and the more active sites for oxidation induced by the larger fraction of interphase boundaries [40].

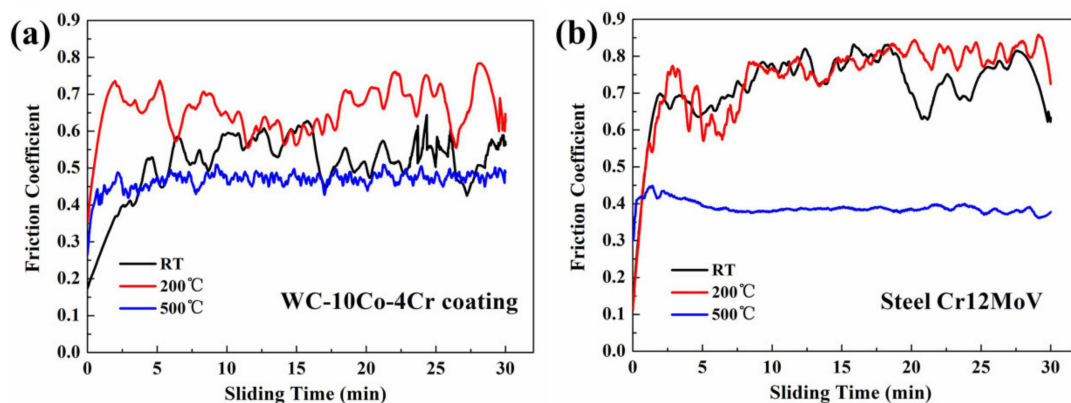


Figure 3. Friction coefficients varied with sliding time for HVOF-sprayed WC-CoCr coatings (a) and Cr12MoV cold work die steel (b) at different temperatures (counterface Al_2O_3 , load 50 N, and sliding velocity $0.9 \text{ m}\cdot\text{s}^{-1}$).

The average values for the friction coefficient during the steady period, R_a , of the worn surfaces and the wear rate are presented in Table 1. There was an approximately 25% increase in the friction coefficient of the coating when test temperature increased from RT to 200 °C. Additionally, it can be observed from Table 1 that the friction coefficient of the coating at 500 °C yielded the lowest friction coefficient value, which was about 29% lower than that at 200 °C. We can deduce that the wear track of the coating at 200 °C had a rougher contact surface and different oxide composition compared to that at RT, and the wear track of the coating at 500 °C appeared to be covered with friction oxide layers as a result of the oxidation of wear debris after the long-term action of high temperature contact between the coating and the Al_2O_3 ceramic. Furthermore, the interposition of the tribo-oxidation film between the coating surface and the Al_2O_3 ceramic ball at 500 °C prevented direct contact and decreased the friction coefficient. The findings in this study are similar to observations in a publication by Bolelli et al. [18], where the dry sliding wear behavior of HVOF-sprayed WC-(W,Cr)₂C-Ni and WC-CoCr hard metal coatings at different temperatures was studied. Wesmann and Espallargas [16] also reported that temperature has a greater effect on friction coefficient than the atmosphere and the carbide size of HVOF-sprayed WC-CoCr coatings. In our study, the average friction coefficients during the steady period of the Cr12MoV cold work die steel at different temperatures were 0.75, 0.79 and 0.38, respectively. It is worth noting that the variation tendency of friction coefficient as a function of temperature for the die steel showed a similar feature, although the reduction of the friction coefficient

from 200 to 500 °C for the die steels was more significant compared to that for the coatings. In addition, the R_a value of worn surface and the wear rate both increased with increasing test temperature for the coatings and the die steels, which suggest that the sliding wear mechanism may be changed at different temperatures. For the coatings, the wear rate increased from $3.58 \times 10^{-5} \text{ mm}^3 \cdot \text{N}^{-1} \cdot \text{m}^{-1}$ at RT to $9.79 \times 10^{-5} \text{ mm}^3 \cdot \text{N}^{-1} \cdot \text{m}^{-1}$ at 500 °C. Similarly for the die steels, the wear rate firstly increased from $9.76 \times 10^{-5} \text{ mm}^3 \cdot \text{N}^{-1} \cdot \text{m}^{-1}$ at RT to $14.39 \times 10^{-5} \text{ mm}^3 \cdot \text{N}^{-1} \cdot \text{m}^{-1}$ at 200 °C, then climbed sharply to $150.4 \times 10^{-5} \text{ mm}^3 \cdot \text{N}^{-1} \cdot \text{m}^{-1}$ at 500 °C. These changes were mainly related to the content and distribution of oxides, as can be seen in detail in undermentioned worn surfaces analysis, as well as to the change of structures and mechanical properties [41]. The second reason for these changes may be that the hardness of the coating increased when test temperature increased from RT to 500 °C, whereas the fracture toughness showed the reverse tendency, resulting in the lowest wear resistance at 500 °C. This is similar to phenomenon reported by Wang et al. [42]. The third reason is the change in contact geometry, which resulted in a low friction coefficient. Moreover, the lubrication regime may have shifted during high temperature sliding, although the formation of tribo-oxidation films was more evident at higher temperature where they covered a larger fraction of the surface.

Table 1. Summary of friction and wear results for WC-10Co-4Cr coatings and Cr12MoV cold work die steel at different temperatures.

Characteristic Parameters	WC-10Co-4Cr Coatings			Cr12MoV Steel		
	RT	200 °C	500 °C	RT	200 °C	500 °C
Average friction coefficient during the steady period	0.53	0.66	0.47	0.75	0.79	0.38
Average surface roughness (R_a) values of worn surfaces, μm	0.13	0.16	0.21	0.28	0.45	2.27
Average wear rate, $10^{-5} \text{ mm}^3 \cdot \text{N}^{-1} \cdot \text{m}^{-1}$	3.58	6.29	9.79	9.76	14.39	150.4

In terms of the comparison between the HVOF-sprayed WC-CoCr coatings and Cr12MoV cold work die steel, the variation of the friction coefficients and wear rates as a function of temperature are shown in Figure 4a,b, respectively. It is clearly shown that the friction coefficients of the die steels were higher than those of the coatings at most test temperatures except at 500 °C (Figure 4a). The notable decrease of the friction coefficient from 200 to 500 °C for the die steels was caused by the absence of pores and oxide inclusions in steel and the formation of compact and smooth oxide films with a self-lubricant function on the surface. For each test temperature, the wear rates of the coatings were consistently lower than those of the die steels, especially at 500 °C (Figure 4b). This is because the coating with the fcc-Co phase and nanocrystalline grains could increase its stabilization, mechanical strength and resistance to plastic flow, therefore resulting in a lower wear rate of the coating at high temperatures. The die steel did not show an improved anti-wear performance at 500 °C, even though it presented the lowest friction coefficient, which can be attributed to the strong plastic deformation and local failure of the materials.

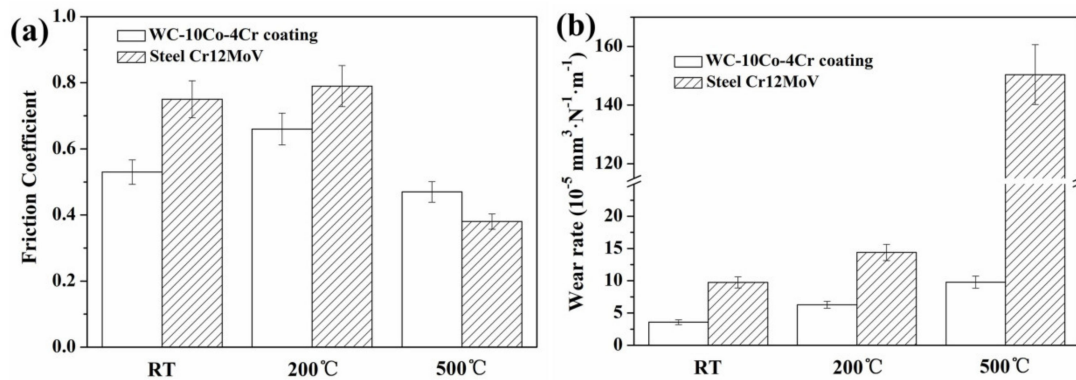


Figure 4. Variation of the friction coefficients (a) and wear rates (b) as a function of temperature for the HVOF-sprayed WC-CoCr coatings and Cr12MoV cold work die steel (counterface Al_2O_3 , load 50 N, sliding velocity $0.9 \text{ m}\cdot\text{s}^{-1}$).

3.3. Worn Surfaces Analysis

After dry sliding against Al_2O_3 ball at different temperatures, the worn surfaces of the HVOF-sprayed WC-CoCr coatings and Cr12MoV cold work die steel were investigated by SEM, ESEM and EDS in order to determine the predominant wear mechanism. Figure 5 presents the SEM images of the worn surfaces of the coatings after 30 min sliding with a load of 50 N and a sliding speed of $0.9 \text{ m}\cdot\text{s}^{-1}$. An examination of the elemental content of non-rubbed surface and different regions of wear scars by the EDS analysis is shown in Table 2. From Figure 5a,b, it can be seen that the worn surface of the coating at RT exhibited relatively smooth characteristics with extrusion deformation sparsely distributed on it. Additionally, small amount of pits and carbide pull-out were detected, demonstrating that severe plastic deformation took place at the carbide–binder interface and cracks initiated at the defects under friction stress. Furthermore, Co, W and O were the primary elements according to the EDS analysis (wt.%) of point A, which suggests a possible formation of oxides. As the test temperature increased to 200 °C, severe wear traces with oxidized clusters could be seen spreading over the worn surface (Figure 5c) as could cracks, carbide pull-out, and adhesion between the coating and the Al_2O_3 ceramic (Figure 5d). The EDS results of point B illustrate a high weight percentage of W and O, confirming that a greater number of oxides were identified on the dark clusters as compared to that at RT. The EDS results of point C demonstrate that W, Al and O appeared on the white debris, although the quantities of the white debris were tiny. The existence of Al content confirms that the adhesive wear phenomenon was formed during the sliding process at 200 °C. The majority of the worn surface of the coating at 500 °C was covered by oxide wear debris and tribo-oxidation film (Figure 5e), which is verified by the EDS analysis of point D in Figure 5f and is consistent with previous studies [43]. The EDS spectrum of point D reveals that the dark grey materials primarily contained Co, W and O. During sliding wear at 500 °C, tribo-oxidation film may have broken up and led to the oxidation of the wear debris when it reached the critical thickness. In addition, wear tracks exhibited cracks and carbide pull-out, along with some regions of fatigue delamination. It is suggested that tribo-oxidation and fatigue wear contributed to the dominant wear mechanism of the coating at 500 °C, resulting in the higher wear rate. As shown in Figure 5 and Table 2, there were light gray areas (labeled as points E, F, and G) on worn surfaces at all test temperatures, and the regions in light gray tone mainly contained W and Co along with the presence of O. Compared with the non-rubbed surface, the content of O on the light gray areas was significantly increased, confirming that slight oxidation occurred along with wear track during sliding wear at all test temperatures, particularly at 500 °C. Moreover, the content of oxygen on the surface rubbed at 200 °C (positions B and C) was higher than those on the surface rubbed at 500 °C (positions D and G), which may have been due to the appearance of adhesive wear as a result of adhesion between the coating and the Al_2O_3 ceramic.

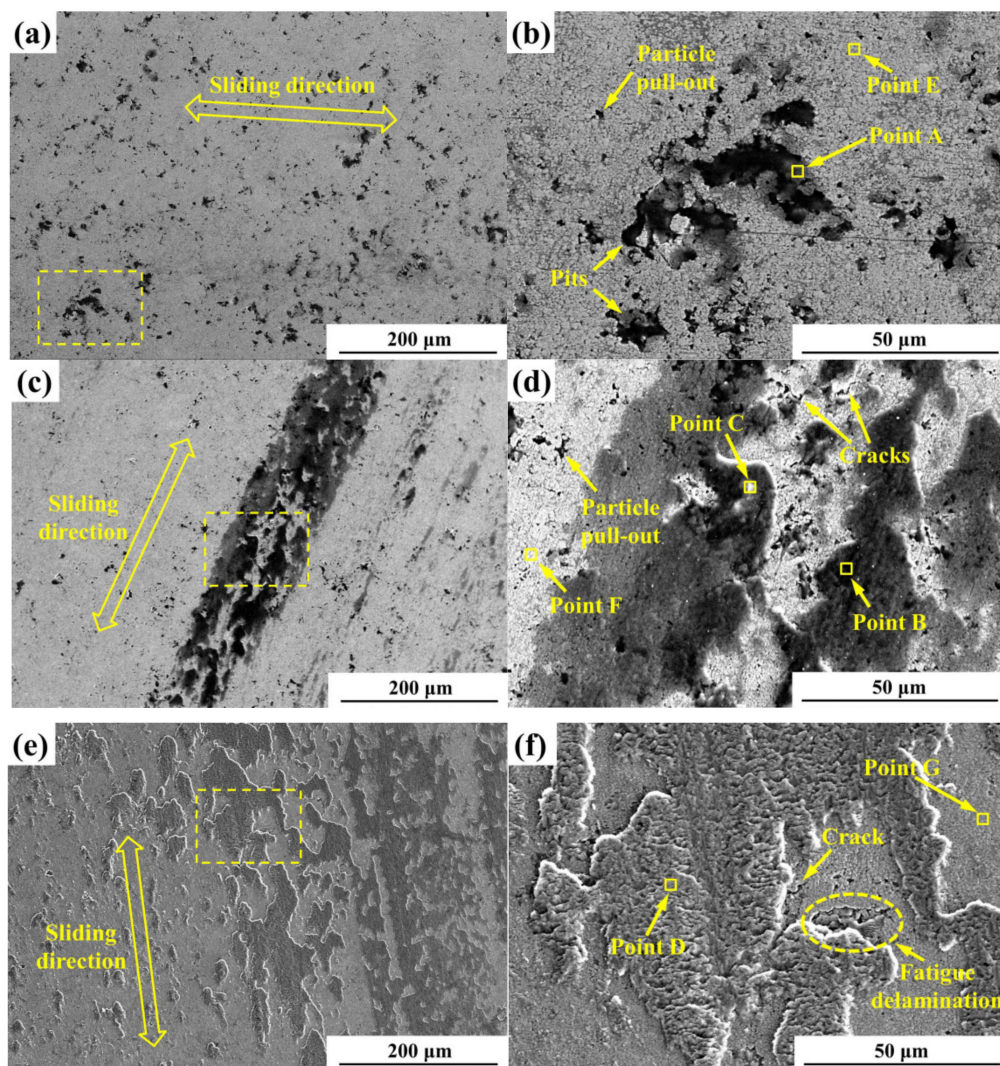


Figure 5. SEM images from worn surfaces of the HVOF-sprayed WC-CoCr coatings at different temperatures: (a,b) room temperature (RT); (c,d) 200 °C; and (e,f) 500 °C. (b) A magnification of the rectangular frame in (a). (d) A magnification of the rectangular frame in (c). (f) A magnification of the rectangular frame in (e).

Table 2. The energy dispersive spectroscopy (EDS) analysis results corresponding to the positions in Figure 5 and the non-rubbed surface.

Element, wt.%	Positions							Non-Rubbed
	A	B	C	D	E	F	G	
C K	1.74	–	1.69	–	10.79	10.10	3.49	21.55
O K	37.95	48.60	32.38	25.58	2.32	5.17	16.15	0.85
Al K	–	–	21.35	–	–	–	–	–
Cr K	2.46	2.99	2.24	2.85	1.59	0.93	2.28	5.30
Co K	8.23	7.37	6.33	8.72	11.05	9.67	11.34	13.96
W K	49.62	41.05	36.01	62.86	74.25	74.13	66.74	58.34

Figure 6 depicts representative ESEM images of worn surfaces of the die steels after 30 min sliding with load of 50 N and a sliding speed of $0.9 \text{ m}\cdot\text{s}^{-1}$. As shown in Figure 6a, a large amount of wear debris in the shape of floccules could be observed on the wear track at RT. This can be explained by the fact that the microhardness of the die steel was $650 \text{ HV}_{0.1}$, well below that of the upper pin of Al_2O_3 ball. At the early stage of sliding, the die steel mainly experienced severe plastic deformation. In the

progress of sliding wear, the forming, expanding and spalling of cracks took place under the stress of extrusion and friction, which led to the formation of wear debris and to the flocculent accumulation of debris. Figure 6b shows that shallow wear grooves, the spalling of carbides and strip-like carbides with the characters of clumped existed on the worn surface of the die steel at 200 °C. This shows that strip-like carbides are capable of withstanding wear grooves to some extent. The reason for this may be that the microhardness of the strip-like carbides (823 HV_{0.1}) was higher than that of the bulk-like carbides (747 HV_{0.1}), which is associated with the enhancement of strength and wear resistance in die steels. In addition, the Cr₇C₃-carbide, as evidenced by XRD analysis in Figure 7b, has a relatively high fracture toughness [44] that contributed to the positive effect on the wear resistance. Wayne et al. [45] found that the higher the fracture toughness, the lower the abrasive wear rate for a range of sintered WC-Co cermet. Huth et al. [46] also reported that M₇C₃-carbides can efficiently deflect wear path. Though the strip-like carbides potentially act as strengthening phases, their spalling is not negligible due to the irregular shape of carbides and the friction stress as the temperature increases, which causes severe abrasive wear and resulted in the growth of the wear rate, as seen in Figure 4b. As the test temperature increased to 500 °C (Figure 6c), a severe plowing phenomenon was observed on the worn surface of the die steel, and this contributed to the extremely high volume loss. Under the combined effect of internal stress, thermal stress, and friction stress, the wear debris and oxides formed furrows on the worn surface as a result of fragmentation and exfoliation, and then the abrasive wear obviously occurred.

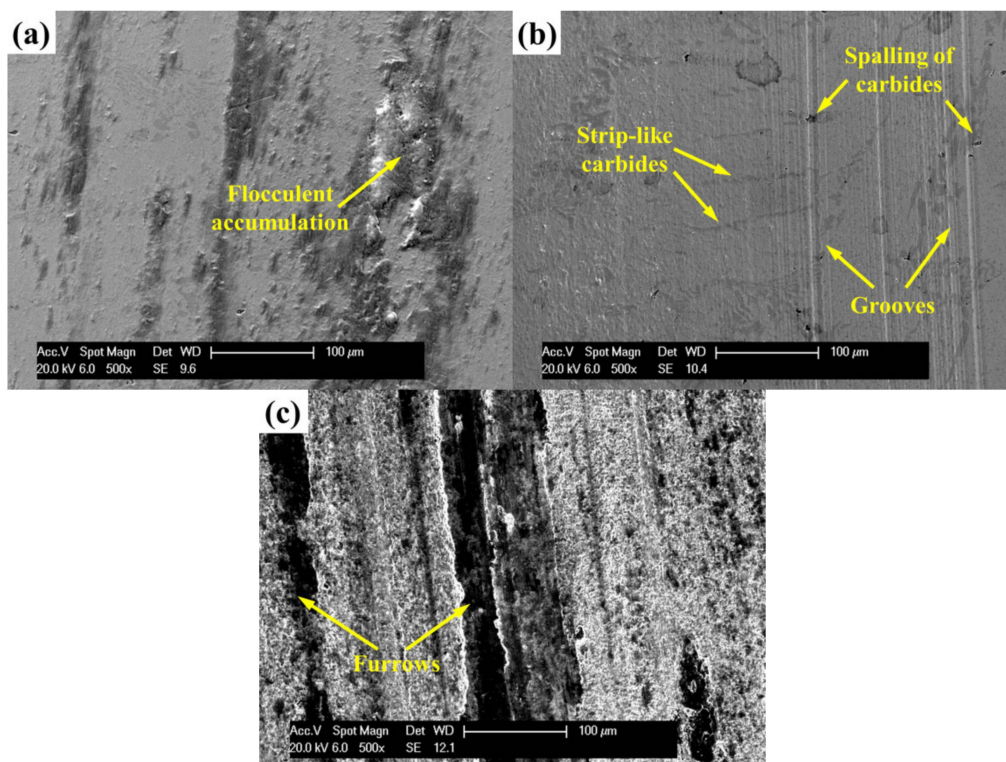


Figure 6. Environmental scanning electron microscopy (ESEM) images from the worn surfaces of Cr12MoV cold work die steel at different temperatures: (a) RT; (b) 200 °C; and (c) 500 °C.

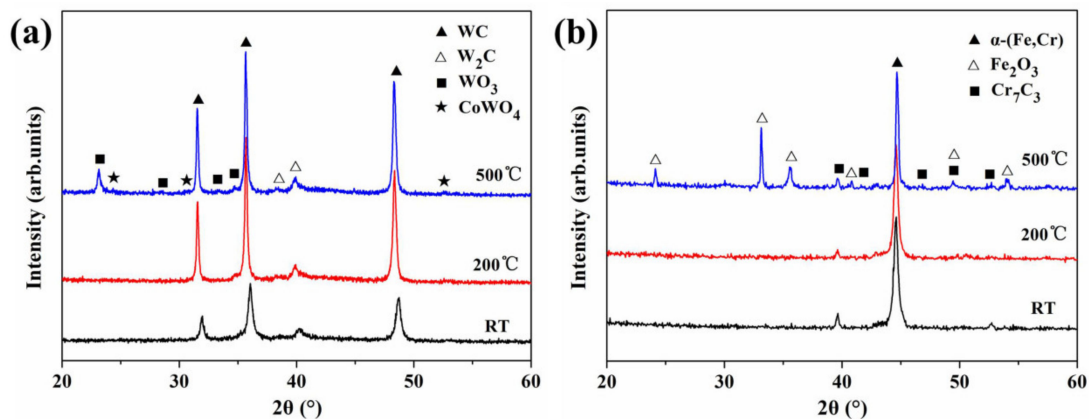


Figure 7. XRD patterns of the worn surface for the HVOF-sprayed WC-CoCr coatings (a) and Cr12MoV cold work die steel (b) at different temperatures (counterface Al_2O_3 , load 50 N, and sliding velocity $0.9 \text{ m}\cdot\text{s}^{-1}$).

The coating and die steel samples were analyzed with XRD to identify and understand the wear mechanisms responsible for the variation of microstructural constituents after the sliding at different temperatures. Figure 7 illustrates the XRD patterns of the worn surfaces of the HVOF-sprayed WC-CoCr coatings and Cr12MoV cold work die steel at different temperatures. The XRD analysis of the coating (Figure 7a) after sliding wear at RT and 200 °C identified the presence of WC and W_2C carbides, as expected when considering the coating composition. In the meanwhile, no evidence of the presence of oxides was found, which suggests that the content of oxides may have been too low to be detected by XRD analysis, and tribo-oxidation was not obvious at relatively low temperature. After sliding wear at 500 °C, WC and W_2C were the main phases, though some additional peaks corresponding to WO_3 alongside some minor CoWO_4 were also identified, suggesting a uniform distribution of oxide phases in the mixture. Comparing the XRD patterns of the coatings at RT and 200 °C, it could be seen that with the increasing test temperature, the intensities of oxide peaks increased (especially the peaks corresponding to WO_3). Similarly for the die steels (Figure 7b), a significant change in the XRD pattern at 500 °C was that new phase of Fe_2O_3 could be identified as compared to those at RT and 200 °C, which indicated the presence of a fraction of the oxide wear debris. Furthermore, the intensities of oxide peaks for the die steel were obviously higher than those for the coating after sliding wear at 500 °C. This may have been because of the presence of the fcc-Co phase (as evidenced in TEM analysis of the coating), whose oxidize rate is relatively low at high temperatures [36,47]. Therefore, the HVOF-sprayed WC-CoCr coating exhibits potential application on Cr12MoV cold work die steel.

4. Conclusions

The experiments were conducted by using HVOF spraying to fabricate a WC-CoCr cermet coating to improve the surface tribological properties of Cr12MoV cold work die steel. The main conclusions can be drawn from this work are as follows:

- (1) The HVOF-sprayed WC-CoCr coating had a dense microstructure and compact interfacial bonding. A nanocrystalline/amorphous structure and an fcc-Co phase could be obtained in this coating, which could increase the mechanical strength, reduce the oxidize rate and maintain the resistance to sliding wear of the coating in comparison with die steel.
- (2) Dry sliding friction and wear tests indicated that the R_a value of the worn surface and the wear rate both increased with increasing test temperature for the coatings and die steels, while the friction coefficient firstly increased as the test temperature increased from RT to 200 °C and then decreased from 200 to 500 °C. For each test temperature, the R_a value of worn surface and the wear rates of the coatings were consistently lower than those of the die steels, especially at 500 °C.

- (3) After the sliding wear at RT and 200 °C for the coating, the presence of oxides was not identified by XRD analysis. The intensities of WO₃ and CoWO₄ peaks increased as the test temperature reached 500 °C. As for the die steels, a new phase of Fe₂O₃ was identified in the XRD pattern at 500 °C as compared to those at RT and 200 °C.
- (4) The tribological properties of coated steel were improved, which could be attributed to its high hardness, low surface roughness, and friction coefficient resulting from the formation of nanocrystalline/amorphous structure and the fcc-Co phase in the coating.
- (5) The sliding wear mechanisms of the coatings were extrusion deformation at RT, carbide pull-out and adhesive wear at 200 °C, and tribo-oxidation wear and fatigue wear at 500 °C. The mechanisms involved in the sliding wear process of the die steels with the increase of the temperature were plastic deformation, the flocculent accumulation of debris, the formation of strip-like carbides, furrows, and abrasive wear.

Author Contributions: Conceptualization, S.H. and Y.W.; Methodology, S.H. and B.W.; Investigation, S.H. and J.L.; Writing—Original Draft Preparation, S.H.; Supervision, S.H. and Y.W.

Funding: The research was supported by the National Natural Science Foundation of China (Grant Nos. 51979083 and 51609067), the Fundamental Research Funds for the Central Universities (Grant No. 2018B17014), the China Postdoctoral Science Foundation (Grant Nos. 2018T110435 and 2017M621665), the Postdoctoral Science Foundation of Jiangsu Province (Grant No. 2018K022A), and Shuangchuang Program of Jiangsu Province.

Conflicts of Interest: The authors declare no conflict of interest.

References

1. Holmberg, K.; Erdemir, A. Influence of tribology on global energy consumption, costs and emissions. *Friction* **2017**, *5*, 263–284. [[CrossRef](#)]
2. Grabon, W.; Pawlus, P.; Wos, S.; Koszela, W.; Wieczorowski, M. Effects of cylinder liner surface topography on friction and wear of liner-ring system at low temperature. *Tribol. Int.* **2018**, *121*, 148–160. [[CrossRef](#)]
3. Szala, M.; Hejwowski, T. Cavitation erosion resistance and wear mechanism model of flame-sprayed Al₂O₃-40%TiO₂/NiMoAl cermet coatings. *Coatings* **2018**, *8*, 254. [[CrossRef](#)]
4. Bayer, I.S. On the durability and wear resistance of transparent superhydrophobic coatings. *Coatings* **2017**, *7*, 12. [[CrossRef](#)]
5. Silva, F.; Martinho, R.; Andrade, M.; Baptista, A.; Alexandre, R. Improving the wear resistance of moulds for the injection of glass fibre-reinforced plastics using PVD coatings: A comparative study. *Coatings* **2017**, *7*, 28. [[CrossRef](#)]
6. Gachot, C.; Rosenkranz, A.; Hsu, S.M.; Costa, H.L. A critical assessment of surface texturing for friction and wear improvement. *Wear* **2017**, *372*, 21–41. [[CrossRef](#)]
7. Tian, L.H.; Feng, Z.K.; Xiong, W. Microstructure, microhardness, and wear resistance of AlCoCrFeNiTi/Ni60 coating by plasma spraying. *Coatings* **2018**, *8*, 112. [[CrossRef](#)]
8. Wang, Y.; Zhao, Y.L.; Darut, G.; Poirier, T.; Stella, J.; Wang, K.; Liao, H.L.; Planche, M.P. A novel structured suspension plasma sprayed YSZ-PTFE composite coating with tribological performance improvement. *Surf. Coat. Technol.* **2019**, *358*, 108–113. [[CrossRef](#)]
9. Singh, J.; Kumar, S.; Mohapatra, S.K. Tribological performance of Yttrium (III) and Zirconium (IV) ceramics reinforced WC-10Co4Cr cermet powder HVOF thermally sprayed on X2CrNiMo-17-12-2 steel. *Ceram. Int.* **2019**, *45*, 23126–23142. [[CrossRef](#)]
10. Singh, J.; Kumar, S.; Mohapatra, S.K. Tribological analysis of WC-10Co-4Cr and Ni-20Cr₂O₃ coating on stainless steel 304. *Wear* **2017**, *376*, 1105–1111. [[CrossRef](#)]
11. Zhang, Y.Q.; Hong, S.; Lin, J.R.; Zheng, Y. Influence of ultrasonic excitation sealing on the corrosion resistance of HVOF-sprayed nanostructured WC-CoCr coatings under different corrosive environments. *Coatings* **2019**, *9*, 724. [[CrossRef](#)]
12. Yuan, J.H.; Ma, C.W.; Yang, S.L.; Yu, Z.S.; Li, H. Improving the wear resistance of HVOF sprayed WC-Co coatings by adding submicron-sized WC particles at the splats' interfaces. *Surf. Coat. Technol.* **2016**, *285*, 17–23. [[CrossRef](#)]

13. Geng, Z.; Hou, S.H.; Shi, G.L.; Duan, D.L.; Li, S. Tribological behaviour at various temperatures of WC-Co coatings prepared using different thermal spraying techniques. *Tribol. Int.* **2016**, *104*, 36–44. [[CrossRef](#)]
14. Da Silva, F.S.; Cinca, N.; Dosta, S.; Cano, I.G.; Couto, M.; Guilemany, J.M.; Benedetti, A.V. Corrosion behavior of WC-Co coatings deposited by cold gas spray onto AA 7075-T6. *Corros. Sci.* **2018**, *136*, 231–243. [[CrossRef](#)]
15. Yang, Q.Q.; Senda, T.; Ohmori, A. Effect of carbide grain size on microstructure and sliding wear behavior of HVOF-sprayed WC–12% Co coatings. *Wear* **2003**, *254*, 23–34. [[CrossRef](#)]
16. Wesmann, J.A.R.; Espallargas, N. Effect of atmosphere, temperature and carbide size on the sliding friction of self-mated HVOF WC-CoCr contacts. *Tribol. Int.* **2016**, *101*, 301–313. [[CrossRef](#)]
17. Mateen, A.; Saha, G.C.; Khan, T.I.; Khalid, F.A. Tribological behaviour of HVOF sprayed near-nanostructured and microstructured WC-17wt.%Co coatings. *Surf. Coat. Technol.* **2011**, *206*, 1077–1084. [[CrossRef](#)]
18. Bolelli, G.; Berger, L.M.; Bonetti, M.; Lusvardi, L. Comparative study of the dry sliding wear behaviour of HVOF-sprayed WC-(W,Cr)₂C-Ni and WC-CoCr hardmetal coatings. *Wear* **2014**, *309*, 96–111. [[CrossRef](#)]
19. Hong, S.; Wu, Y.P.; Wang, B.; Zheng, Y.G.; Gao, W.W.; Li, G.Y. High-velocity oxygen-fuel spray parameter optimization of nanostructured WC-10Co-4Cr coatings and sliding wear behavior of the optimized coating. *Mater. Des.* **2014**, *55*, 286–291. [[CrossRef](#)]
20. Qiao, Y.F.; Fischer, T.E.; Dent, A. The effects of fuel chemistry and feedstock powder structure on the mechanical and tribological properties of HVOF thermal-sprayed WC-Co coatings with very fine structures. *Surf. Coat. Technol.* **2003**, *172*, 24–41. [[CrossRef](#)]
21. Basak, A.K.; Celis, J.P.; Vardavoulias, M.; Matteazzi, P. Effect of nanostructuring and Al alloying on friction and wear behaviour of thermal sprayed WC-Co coatings. *Surf. Coat. Technol.* **2012**, *206*, 3508–3516. [[CrossRef](#)]
22. Rovatti, L.; Lecis, N.; Dellasega, D.; Russo, V.; Gariboldi, E. Influence of aging in the temperature range 250–350 °C on the tribological performance of a WC-CoCr coating produced by HVOF. *Int. J. Refract. Met. Hard Mater.* **2018**, *75*, 218–224. [[CrossRef](#)]
23. Hong, S.; Wu, Y.P.; Wang, B.; Zhang, J.F.; Zheng, Y.; Qiao, L. The effect of temperature on the dry sliding wear behavior of HVOF sprayed nanostructured WC-CoCr coatings. *Ceram. Int.* **2017**, *43*, 458–462. [[CrossRef](#)]
24. Wu, Y.P.; Wang, B.; Hong, S.; Zhang, J.F.; Qin, Y.J.; Li, G.Y. Dry sliding wear properties of HVOF sprayed WC-10Co-4Cr coating. *Trans. Indian Inst. Metals* **2015**, *68*, 581–586. [[CrossRef](#)]
25. ASTM G99-05 Standard Test Method for Wear Testing with a Pin-on-Disk Apparatus; ASTM International: West Conshohocken, PA, USA, 2010.
26. Hong, S.; Wu, Y.P.; Gao, W.W.; Wang, B.; Guo, W.M.; Lin, J.R. Microstructural characterisation and microhardness distribution of HVOF sprayed WC-10Co-4Cr coating. *Surf. Eng.* **2014**, *30*, 53–58. [[CrossRef](#)]
27. Hong, S.; Wu, Y.P.; Gao, W.W.; Zhang, J.F.; Zheng, Y.G.; Zheng, Y. Slurry erosion-corrosion resistance and microbial corrosion electrochemical characteristics of HVOF sprayed WC-10Co-4Cr coating for offshore hydraulic machinery. *Int. J. Refract. Met. Hard Mater.* **2018**, *74*, 7–13. [[CrossRef](#)]
28. Schwetzke, R.; Kreye, H. Microstructure and properties of tungsten carbide coatings sprayed with various High-velocity oxygen fuel spray systems. *J. Therm. Spray Technol.* **1999**, *8*, 433–439. [[CrossRef](#)]
29. Niu, Y.R.; Zheng, X.B.; Ji, H.; Qi, L.J.; Ding, C.X.; Chen, J.L.; Luo, G.N. Microstructure and thermal property of tungsten coatings prepared by vacuum plasma spraying technology. *Fusion Eng. Des.* **2010**, *85*, 1521–1526. [[CrossRef](#)]
30. Stewart, D.A.; Shipway, P.H.; McCartney, D.G. Microstructural evolution in thermally sprayed WC-Co coatings: Comparison between nanocomposite and conventional starting powders. *Acta Mater.* **2000**, *48*, 1593–1604. [[CrossRef](#)]
31. Li, C.J.; Ohmori, A.; Harada, Y. Formation of an amorphous phase in thermally sprayed WC-Co. *J. Therm. Spray Technol.* **1996**, *5*, 69–73. [[CrossRef](#)]
32. Jiang, N.; Shen, Y.G.; Mai, Y.W.; Chan, T.; Tung, S.C. Nanocomposite Ti-Si-N films deposited by reactive unbalanced magnetron sputtering at room temperature. *Mater. Sci. Eng. B* **2004**, *106*, 163–171. [[CrossRef](#)]
33. Lee, K.H.; Chang, D.; Kwon, S.C. Properties of electrodeposited nanocrystalline Ni-B alloy films. *Electrochim. Acta* **2005**, *50*, 4538–4543. [[CrossRef](#)]
34. Sobolev, V.V.; Guilemany, J.M.; Miguel, J.R.; Calero, J.A. Investigation of the development of coating structure during high velocity oxy-fuel (HVOF) spraying of WC-Ni powder particles. *Surf. Coat. Technol.* **1996**, *82*, 114–120. [[CrossRef](#)]

35. Sharma, P.; Majumdar, J.D. Surface characterization and mechanical properties evaluation of Boride-dispersed Nickel-based coatings deposited on copper through thermal spray routes. *J. Therm. Spray Technol.* **2012**, *21*, 800–809. [[CrossRef](#)]
36. Human, A.M.; Roebuck, B.; Exner, H.E. Electrochemical polarisation and corrosion behaviour of cobalt and Co (W, C) alloys in 1 N sulphuric acid. *Mater. Sci. Eng. A* **1998**, *241*, 202–210. [[CrossRef](#)]
37. Blau, P.J. *Friction and Wear Transitions of Materials*; Noyes Publishing: Park Ridge, NJ, USA, 1989.
38. Zhu, Y.C.; Yukimura, K.; Ding, C.X.; Zhang, P.Y. Tribological properties of nanostructured and conventional WC-Co coatings deposited by plasma spraying. *Thin Solid Films* **2001**, *388*, 277–282. [[CrossRef](#)]
39. Wu, L.; Chen, J.X.; Liu, M.Y.; Bao, Y.W.; Zhou, Y.C. Reciprocating friction and wear behavior of Ti₃AlC₂ and Ti₃AlC₂/Al₂O₃ composites against AISI52100 bearing steel. *Wear* **2009**, *266*, 158–166. [[CrossRef](#)]
40. Lekatou, A.; Sioulas, D.; Karantzalis, A.E.; Grimanelis, D. A comparative study on the microstructure and surface property evaluation of coatings produced from nanostructured and conventional WC-Co powders HVOF-sprayed on Al7075. *Surf. Coat. Technol.* **2015**, *276*, 539–556. [[CrossRef](#)]
41. Shipway, P.H.; McCartney, D.G.; Sudaprasert, T. Sliding wear behaviour of conventional and nanostructured HVOF sprayed WC-Co coatings. *Wear* **2005**, *259*, 820–827. [[CrossRef](#)]
42. Wang, Q.; Li, L.X.; Yang, G.B.; Zhao, X.Q.; Ding, Z.X. Influence of heat treatment on the microstructure and performance of high-velocity oxy-fuel sprayed WC–12Co coatings. *Surf. Coat. Technol.* **2012**, *206*, 4000–4010. [[CrossRef](#)]
43. Geng, Z.; Li, S.; Duan, D.L.; Liu, Y. Wear behavior of WC-Co HVOF coatings at different temperatures in air and argon. *Wear* **2015**, *330*, 348–353. [[CrossRef](#)]
44. Guo, J.; Ai, L.Q.; Wang, T.T.; Feng, Y.L.; Wan, D.C.; Yang, Q.X. Microstructure evolution and micro-mechanical behavior of secondary carbides at grain boundary in a Fe-Cr-W-Mo-V-C alloy. *Mater. Sci. Eng. A* **2018**, *715*, 359–369. [[CrossRef](#)]
45. Wayne, S.F.; Baldoni, J.G.; Buljan, S.T. Abrasion and erosion of WC-Co with controlled microstructures. *Tribol. Trans.* **1990**, *33*, 611–617. [[CrossRef](#)]
46. Huth, S.; Krasokha, N.; Theisen, W. Development of wear and corrosion resistant cold-work tool steels produced by diffusion alloying. *Wear* **2009**, *267*, 449–457. [[CrossRef](#)]
47. Zhang, Y.Q.; Li, C.Y.; Xu, Y.H.; Tang, Q.H.; Zheng, Y.; Liu, H.W.; Fernandez-Rodriguez, E. Study on propellers distribution and flow field in the oxidation ditch based on two-phase CFD model. *Water* **2019**, *11*, 2506. [[CrossRef](#)]



© 2019 by the authors. Licensee MDPI, Basel, Switzerland. This article is an open access article distributed under the terms and conditions of the Creative Commons Attribution (CC BY) license (<http://creativecommons.org/licenses/by/4.0/>).